INTERNATIONAL JOURNAL FOR NUMERICAL METHODS IN FLUIDS, VOL. 20, 1253–1262 (1995)

# TRANSLATION OF A SPHERE IN A ROTATING VISCOUS FLUID: A NUMERICAL STUDY

C. V. RAGHAVA RAO AND T. V. S. SEKHAR

*Department of Mathematics, Indian Institute of Technology, Madras 600 036, India*

SUMMARY

The translation of a sphere moving along the axis of a rotating viscous fluid is studied by the finite difference method at moderate Reynolds (up to $R = 500$) and Taylor (up to $T = 100$) numbers. Suppression of the separation is observed with increasing rotation parameter $T$. The drag coefficient is also presented. It is observed that the drag coefficient is less than that with no rotation in the range $0 < N < 0{\cdot}7$, where $N = 2T/R$ is the inverse Rossby number. The same phenomenon was observed experimentally by Maxworthy in the range $0 < N < 0{\cdot}75 \pm 0{\cdot}03$.

KEY WORDS rotating fluid; suppression; separation; slug; finite difference method

## INTRODUCTION

Taylor[1] found that as a sphere moved slowly through a fluid in solid body rotation, a column of fluid was pushed ahead of the sphere as a "slug' of zero axial velocity relative to the body. In the limit of zero axial viscosity this column was presumed to become a cylinder, extending ahead of and behind the body, with generators parallel to the axis of rotation and just touching the largest cross-section of the body. What he saw was presumed to be the viscous modification of an ideal flow. Taylor reported that this behaviour appeared only when the parameter $N = 2\omega a/U_\infty$ exceeded a magnitude of about $N = 6$. Here $\omega$ is the angular velocity of the fluid in solid body rotation and $U_\infty$ and $a$ are the velocity and radius of the sphere respectively. Further observations by Long[2] demonstrated the existence of a train of waves downstream of the disturbing body when $N$ was small. They apparently disappeared as $N$ approached the slug flow regime. Again there were visualizations of slug flow ahead of the body and a strong cyclonic vortex behind.

Maxworthy[3] performed experiments in a small rotating tank and verified the existence of the forward slug. It did not disappear when $N < 6$. It was much in evidence for $N \approx 2$ but in a modified form. He also observed a rearward slug at large $N$. He reported that for small values of $N$ it rotated rapidly, had an oscillatory character, was much longer than the forward slug and completely modified the separation bubble that normally exists at the Reynolds numbers of the experiments. He also observed that at low $N$ the drag is less than that with no rotation in the range $0 < N < 0{\cdot}75 \pm 0{\cdot}03$, independently of $T$. For intermediate ranges of $T$ and $N$ Maxworthy observed that the drag is greater than that with no rotation.

Recently Raghava Rao and Sekhar[4] obtained forward separation of the axisymmetric flow past a sphere moving in a rotating fluid with the formation of an upstream separation bubble, such as observed by Maxworthy[3] and Miles,[5] by using the finite difference method. They also found a vortex

CCC 0271–2091/95/111253–10

*Received February 1994*
*Revised October 1994*

phenomenon at the rear stagnation point. For small values of $R$ and moderate values of $T$ a finite difference solution giving the flow past a stationary and spinning sphere in a rotating fluid has been obtained by Raghava Rao and Sekhar.[6] A region of reverse flow and vortex formation is found to occur near the front or rear stagnation point or both depending upon the values of $R$ and $T$ and the angular velocity of the sphere.

In this present investigation the translation of a sphere in a rotating fluid is considered for moderate Reynolds and Taylor numbers.

## FORMULATION OF THE PROBLEM

In this paper we study the steady flow of a viscous incompressible fluid past a sphere of radius $a$ which is moving with a uniform translational velocity $U$. The undisturbed fluid rotates with constant angular velocity $\omega_0$ and the axis of rotation is taken to coincide with the line of motion. We use spherical polar co-ordinates $(r, \theta, \phi)$ with the origin at the centre of the sphere; since the motion is axially symmetric about the $z$-axis, all quantities are independent of $\phi$. The velocity components $(v_r^*, v_\theta^*, v_\phi^*)$ are related to the streamfunction $\psi^*$ and the rotational velocity component $\Omega^*$ by the relations

$$v_r^* = \frac{1}{r^2 \sin\theta}\frac{\partial \psi^*}{\partial \theta}, \qquad v_\theta^* = \frac{1}{r \sin\theta}\frac{\partial \psi^*}{\partial r}, \qquad v_\phi^* = \frac{\Omega^*}{r \sin\theta}.$$

$\psi^*$ and $\Omega^*$ are non-dimensionalized as

$$\psi^* = a^2 U \psi, \qquad \Omega^* = a^2 \omega_0 \Omega,$$

while non-dimensional velocity components $(v_r, v_\theta, v_\phi)$ are obtained by dividing the dimensional components $v_r^*$ and $v_\theta^*$ by $U$ and $v_\phi^*$ by $a\omega_0$. If we put $r = e^\xi$, we obtain for the velocity components

$$V_r = \frac{e^{-2\xi}}{\sin\theta}\frac{\partial \psi}{\partial \theta}, \qquad V_\theta = -\frac{e^{-\xi}}{\sin\theta}\frac{\partial \psi}{\partial \xi}, \qquad V_\phi = \frac{\Omega e^{-\xi}}{\sin\theta}.$$

The Navier–Stokes equations governing the motion are

$$D^2\Omega = \frac{Re^{-\xi}}{\sin\theta}\left(\frac{\partial \psi}{\partial \theta}\frac{\partial \Omega}{\partial \xi} - \frac{\partial \psi}{\partial \xi}\frac{\partial \Omega}{\partial \theta}\right), \tag{1}$$

$$D^2\psi = -e^{2\xi}\zeta, \tag{2}$$

$$D^2\zeta = \frac{Re^{-\xi}}{\sin\theta}\left[\left(\frac{\partial \psi}{\partial \theta}\frac{\partial \zeta}{\partial \xi} - \frac{\partial \psi}{\partial \xi}\frac{\partial \zeta}{\partial \theta}\right) + 2\left(\cot\theta\frac{\partial \psi}{\partial \xi} - \frac{\partial \psi}{\partial \theta}\right)\zeta - \frac{2T^2}{R^2}\left(\cot\theta\frac{\partial \Omega}{\partial \xi} - \frac{\partial \Omega}{\partial \theta}\right)\Omega\right], \tag{3}$$

where

$$D^2 = \frac{\partial^2}{\partial \xi^2} - \frac{\partial}{\partial \xi} + \sin\theta\frac{\partial}{\partial \theta}\left(\frac{1}{\sin\theta}\frac{\partial}{\partial \theta}\right)$$

and $\psi$, $\Omega e^{-\xi}/\sin\theta$ and $\zeta e^{-\xi}/\sin\theta$ are the dimensionless streamfunction, angular velocity and vorticity respectively. The boundary conditions are

$$\Omega = 0, \quad \psi = 0, \quad \frac{\partial \psi}{\partial \xi} = 0, \quad \text{at } \xi = 0,$$

$$\Omega \sim e^{2\xi}\sin^2\theta, \quad \psi \sim \tfrac{1}{2}e^{2\xi}\sin^2\theta, \quad \zeta \to 0 \quad \text{as} \quad \xi \to \xi_\infty, \quad 0 \le \theta \le \pi.$$

## NUMERICAL METHOD

The finite difference method is used to solve the governing equations. The finite difference grid is shown in Figure 1, where $\xi$ = constant are circles, $\theta$ = constant are radial lines and nodal points are the points of intersection of these circles and radial lines. The central difference approximation to the governing equations requires severe underrelaxation for convergence when solving the finite difference equations by iterative techniques. The use of upwind differences in approximating the non-linear terms ensures diagonal dominance, which in turn ensures the convergence of the iterative procedure even at high Reynolds numbers. In the present study, second-order derivatives are approximated by central differences and non-linear terms are approximated by an upwind difference scheme which can be written as

$$(F_\theta \cdot f_\xi) = 0{\cdot}5\left[(F_\theta + |F_\theta|)(f_{i,j} - f_{i-1,j}) + (F_\theta - |F_\theta|)(f_{i+1,j} - f_{i,j})\right],$$

where $f = \Omega$ or $\zeta$, $F = \psi$, $F_\theta = \partial F/\partial\theta$ and $f_\xi = \partial f/\partial\xi$. If $F_\theta > 0$, $f_\xi$ is approximated by backward differences; if $F_\theta < 0$, $f_\xi$ is approximated by forward differences and $F_\theta$ is approximated by central differences. The coupled equations are solved by the block SLOR method and the resulting algebraic equations are solved by the SOR method. The initial solution is taken as $\psi = 0$, $\zeta = 0$ and $\Omega = 0$ at all inner grid points. In finding the solutions for higher values of $R$ and $T$, the solutions obtained for lower values of $R$ and $T$ are used as starting solutions. Without resorting to underrelaxation, we could apply the Gauss–Seidel iterative method for the Reynolds numbers $R = 5$, 20 and 40 for all values of the Taylor number $T$. Numerical solutions have been obtained for the values of the parameters given in Table I.

The order of the solution procedure is as follows. First we solve equation (1) for $\Omega$, then, using this in equation (3), we solve for $\zeta$; finally, this is used to solve equation (2) for $\psi$. This completes one iteration. The above procedure is repeated until it satisfies the equation

$$\left|f^{(n+1)} - f^{(n)}\right| \leq 0.0001,$$

where $f = \psi$, $\zeta$ or $\Omega$ and $n$ is the iteration number, at all interior grid points.

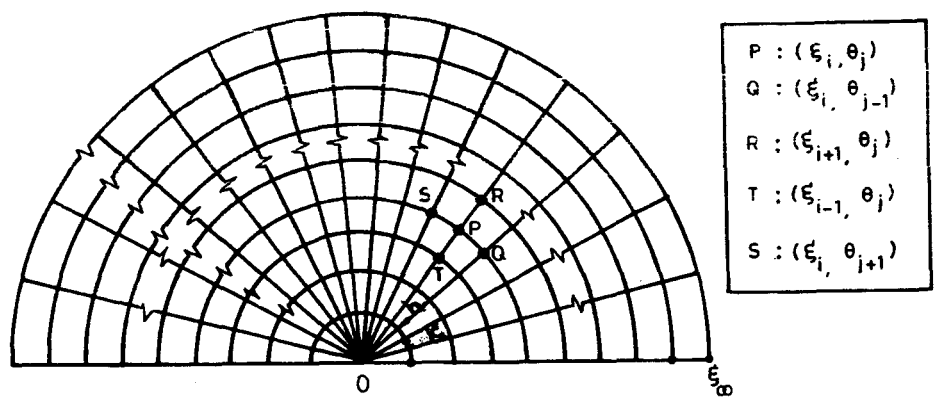


Figure 1. Finite difference grid

Table I. Parameters used in the calculations

| $R$ | $T$ | $h$ | $k$ | $\xi_m$ | Relaxation parameter |
|---|---|---|---|---|---|
| 5 | 0, 0·5, 1, 2, 2·5 | 0·05 | $\pi/45$ | 2·05 | No relaxation parameter |
| 20 | 0, 5 | 0·05 | $\pi/45$ | 2·05 | No relaxation parameter |
| 40 | 0, 5, 8, 12 | 0·05 | $\pi/45$ | 2·05 | No relaxation parameter |
| 100 | 0, 10, 20 | 0·05 | $\pi/60$ | 2·5 | 1, 0·8, 0·5 |
| 500 | 0, 40, 60, 100 | 0·05 | $\pi/60$ | 2·5 | 1, 0·8, 0·5, 0·4 |

## RESULTS

The flow is studied first in the case of $T = 0$ and then upon increasing the value of $T$ (Figures 2–12). In the case of $T = 0$ the separation starts at $R = 20$ (Figure 2(a)) and the length of the wake grows slowly with increasing $R$ (Figures 4(a), 7(a) and 9(a)) as found by Fornberg.[7] Many interesting features are observed at moderate values of the Taylor number.

The wake which is found in the case of $T = 0$ disappears slowly as the rotation parameter $T$ increases. At $R = 20$ and 40 the wake completely disappears at $T = 5$ and 12 respectively (Figures 3(a) and 6(a)). This phenomenon has been observed in the magnetohydrodynamic flow past a circular cylinder by several authors.[8–11] At $R = 100$ suppression of the separation is also seen (Figures 7(a) and 8(a)). At $R = 500$ and $T = 60$ the separation is completely modified as a vortex which is attached to the body (Figure 11(a)), and as $T$ increases, this vortex moves upwards (Figure 12(a)).

The drag coefficient $C_D$ is the sum of two components: one arising from the viscous force ($C_V$) and the other from the pressure distribution over the sphere ($C_P$). These components can be written in polar co-ordinates $(r, \theta)$ as

$$C_V = -\frac{4}{R}\int_0^{\pi} \zeta_{r=1} \sin^2\theta \, d\theta,$$

$$C_P = \frac{2}{R}\int_0^{\pi} \left(\zeta + \frac{\partial \zeta}{\partial r}\right)_{r=1} \sin^2\theta \, d\theta.$$

The drag coefficient is calculated for $R = 5$, 20 and 40 in the range $0 \leq N \leq 0{\cdot}7$, and for $R = 100$ and 500 in the range $0 \leq N \leq 0{\cdot}4$ (Figure 13). It is found that the drag coefficient is less than that with no rotation in the range $0 < N < 0{\cdot}7$ (see Tables II–VI for drag coefficients), independently of $T$. The same phenomenon was observed by Maxworthy[3] in the range $0 < N < 0{\cdot}75 \pm 0{\cdot}03$, independently of $T$. This result can be explained physically by considering a weakly rotating fluid flowing over the sphere plus a rear recirculation region similar in shape to that in a non-rotating fluid, i.e. viscous separation takes place before the equator and the bubble has a larger transverse dimension than the sphere. The outward flow of rotating fluid over this bubble causes it to rotate at a rate less than the applied value, the pressure in the bubble increases and the drag on the body decreases. For $N \geq 0{\cdot}7$ the drag coefficient is greater than that with no rotation (within the range of our observations). The values of the drag coefficients ($C_D$) and angles of separation ($\theta_s$) are given in Tables II–VI.

The effect of the infinite distance is studied in the case of $T = 0$ for $R = 20$, 40 and 500. The values of the drag coefficients for various $\xi_\infty$ are given in Table VII.

It may be noticed from Table VII that as $\xi_\infty$ increases, the present results for $T = 0$ become closer to the results given in References 7, 12 and 13. However, it may also be noticed from Table 8 that a

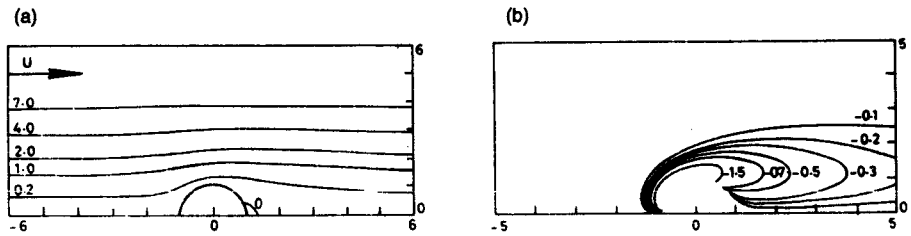


Figure 2. (a) Streamlines and (b) vorticity lines at $R = 20$, $T = 0$

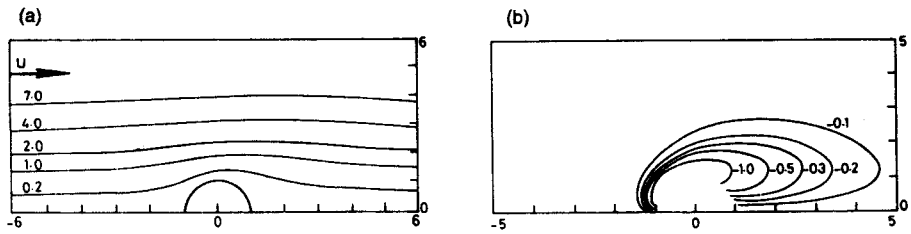


Figure 3. (a) Streamlines and (b) vorticity lines at $R = 20$, $T = 5$

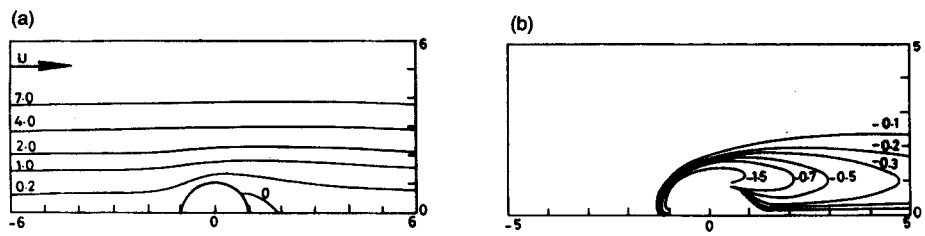


Figure 4. (a) Streamlines and (b) vorticity lines at $R = 40$, $T = 0$

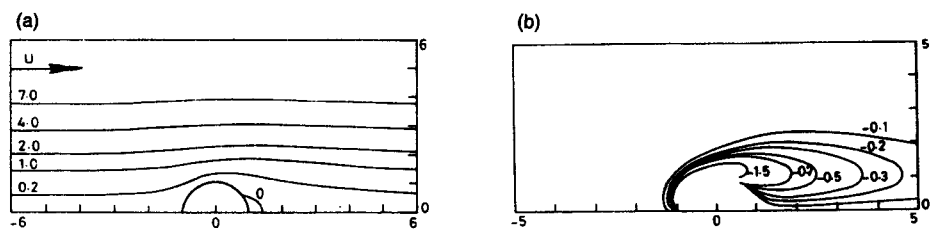


Figure 5. (a) Streamlines and (b) vorticity lines at $R = 40$, $T = 8$

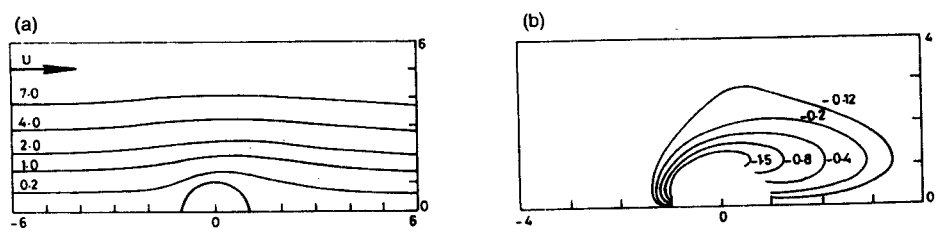


Figure 6. (a) Streamlines and (b) vorticity lines at $R = 40$, $T = 12$

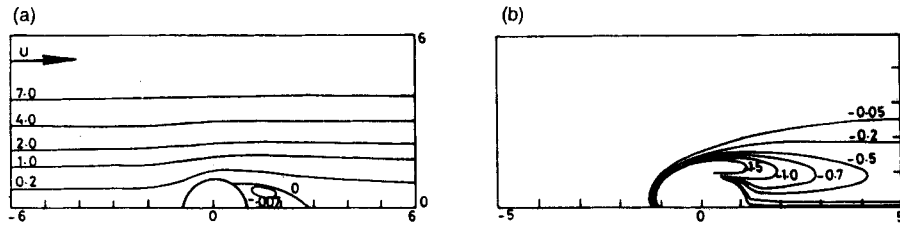


Figure 7. (a) Streamlines and (b) vorticity lines at $R = 100$, $T = 0$

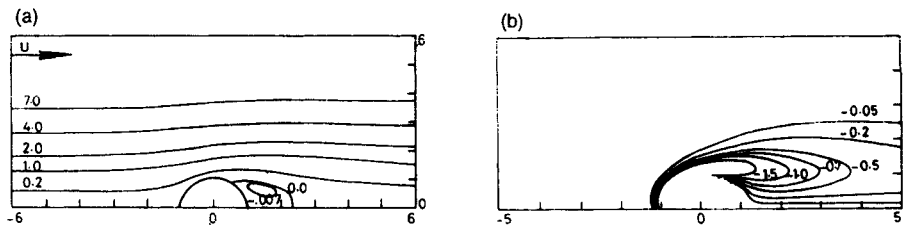


Figure 8. (a) Streamlines and (b) vorticity lines at $R = 100$, $T = 20$

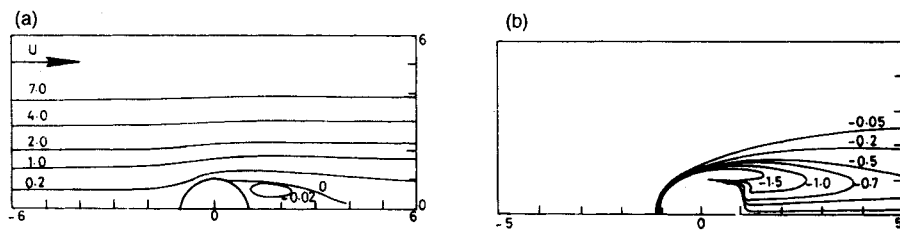


Figure 9. (a) Streamlines and (b) vorticity lines at $R = 500$, $T = 0$

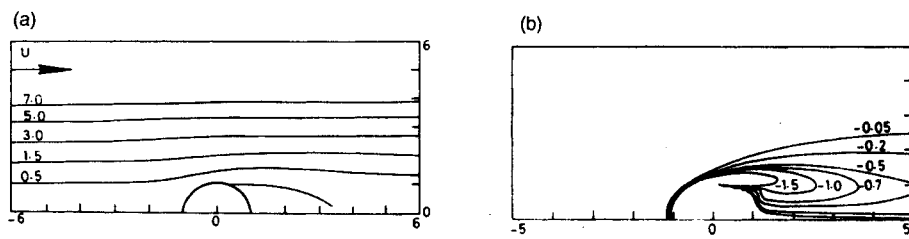


Figure 10. (a) Streamlines and (b) vorticity lines at $R = 500$, $T = 40$

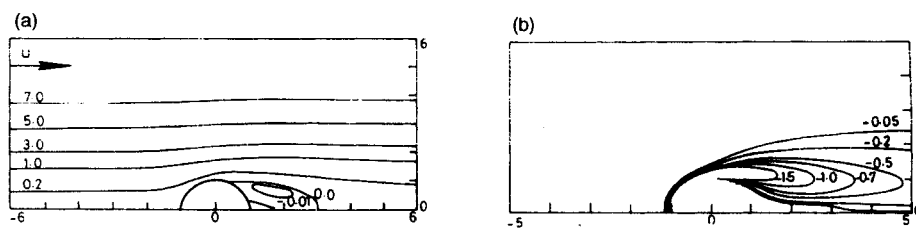


Figure 11. (a) Streamlines and (b) vorticity lines at $R = 500$, $T = 60$

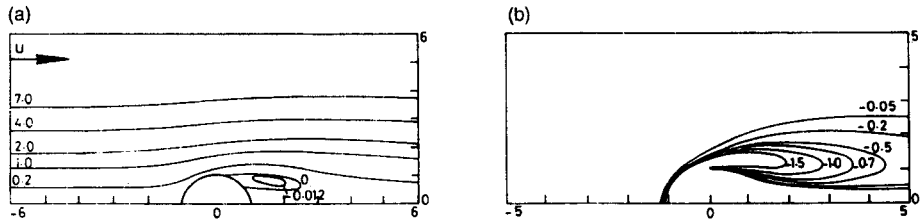


Figure 12. (a) Streamlines and (b) vorticity lines at $R = 500$, $T = 100$

Table II. $R = 5$, $\xi_\infty = 2{\cdot}05$

| $T$ | $N$ | $\theta_s$ (deg) | $C_D$ | Jenson[12] | Dennis and Walker[13] |
|---|---|---|---|---|---|
| 0 | 0 | — | 4·5621 | 3·975 | 3·605 |
| 0·5 | 0·2 | — | 4·4686 | — | — |
| 1 | 0·4 | — | 4·1870 | — | — |
| 1·5 | 0·6 | — | 3·8777 | — | — |
| 1·75 | 0·7 | — | 4·0336 | — | — |
| 2 | 0·8 | — | 4·4949 | — | — |
| 2·5 | 1 | — | 5·7307 | — | — |

Table III. $R = 20$, $\xi_\infty = 2{\cdot}05$

| $T$ | $N$ | $\theta_s$ (deg) | $C_D$ | Jenson[12] | Dennis and Walker[13] |
|---|---|---|---|---|---|
| 0 | 0 | 24 | 1·7796 | 1·473 | 1·365 |
| 2 | 0·2 | 20 | 1·7382 | — | — |
| 5 | 0·5 | — | 1·4902 | — | — |
| 6 | 0·6 | — | 1·3332 | — | — |
| 7 | 0·7 | — | 1·4291 | — | — |

Table IV. $R = 40$, $\xi_\infty = 2{\cdot}05$

| $T$ | $N$ | $\theta_s$ (deg) | $C_D$ | Jenson[12] | Dennis and Walker[13] |
|---|---|---|---|---|---|
| 0 | 0 | 36 | 1·1434 | 0·931 | 0·904 |
| 8 | 0·4 | 32 | 1·0240 | — | — |
| 10 | 0·5 | — | 0·9467 | — | — |
| 12 | 0·6 | — | 0·8322 | — | — |
| 14 | 0·7 | — | 0·9305 | — | — |

Table V. $R = 100$, $\xi_\infty = 2{\cdot}5$

| $T$ | $N$ | $\theta_s$ (deg) | $C_D$ | Fornberg[7] |
|---|---|---|---|---|
| 0 | 0 | 51 | 0·5953 | 0·54 |
| 5 | 0·1 | 51 | 0·5932 | — |
| 10 | 0·2 | 51 | 0·5890 | — |
| 20 | 0·4 | 57 | 0·4937 | — |

Table VI. $R = 500$, $\xi_\infty = 2{\cdot}5$

| $T$ | $N$ | $\theta_s$ (deg) | $C_D$ | Fornberg[7] |
|---|---|---|---|---|
| 0 | 0 | 66 | 0·2682 | 0·24 |
| 40 | 0·16 | 66 | 0·2662 | — |
| 60 | 0·24 | 18, 69 | 0·2617 | — |
| 100 | 0·4 | 36, 75 | 0·2198 | — |

Table VII. Drag coefficients for various $\xi_\infty$

| $R$ | $\xi_\infty = 2{\cdot}05$ | $\xi_\infty = 2{\cdot}5$ $k = \pi/60$ | $\xi_\infty = 2{\cdot}75$ $k = \pi/60$ | $\xi_\infty = 3{\cdot}0$ $k = \pi/60$ |
|---|---|---|---|---|
| 20 | 1·7796 | 1·7278 | — | — |
| 40 | 1·1434 | 1·1047 | — | — |
| 500 | — | 0·2682 | 0·2627 | 0·2588 |

Table VIII. Variation in $C_D$ for $R = 40$ with the position of the outer boundary conditions at various values of $T$

| $\xi_\infty$ | $T=4$ | $T=5$ | $T=6$ |
|---|---|---|---|
| 2·05 | 1·1130 | 1·0970 | 1·0791 |
| 2·25 | 1·0935 | 1·0809 | 1·0630 |
| 2·5 | 1·0944 | 1·0892 | 1·0825 |

smaller value of $\xi_\infty$ is needed to obtain satisfactory results as $T$ increases, which is also mentioned by Dennis *et al.*[14] for $R = 0{\cdot}12$ and $T = 0{\cdot}12$, $0{\cdot}25$ and $0{\cdot}5$. In the present investigation we could not go beyond $N > 0{\cdot}4$ for $R = 100$ and 500 since we could not get the required convergence of $10^{-4}$. The values of the drag coefficients for $N = 0{\cdot}5$, $0{\cdot}6$ and $0{\cdot}7$ at $R = 100$ and 500 are extrapolated by using Newton's backward interpolation formula to draw the graphs between $R$ and $C_D$ for different $N$ (see Figure 13). From Figures 11(a) and 12(a) it is clear that the lower separation point moves faster than the upper separation point. Thus, as $N$ increases further, these separation points may coincide with each other, and as $N$ increases further still, this "combined' separation point may even detach from the body. The vorticity on the surface of the sphere is shown in Figures 14 and 15 for $R = 40$ and 500 respectively.

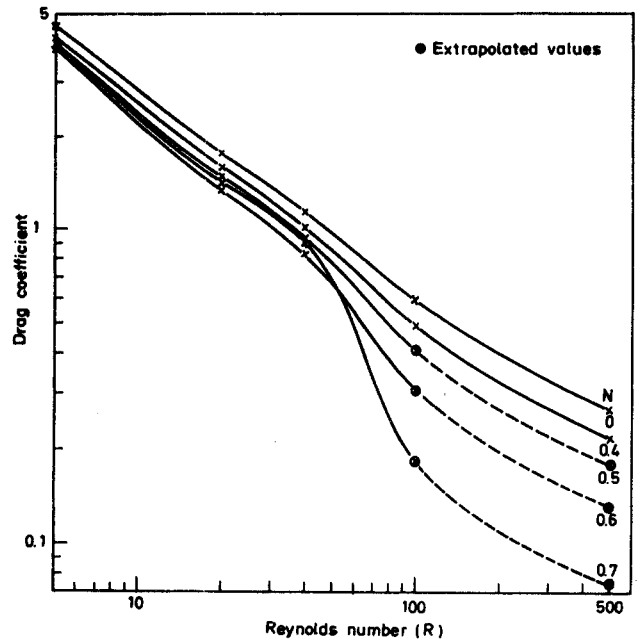


Figure 13. Drag coefficient versus Reynolds number

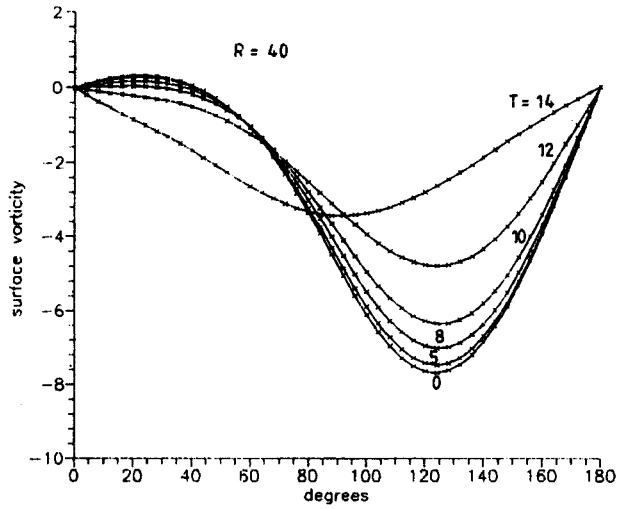


Figure 14. Surface vorticity at $R = 40$

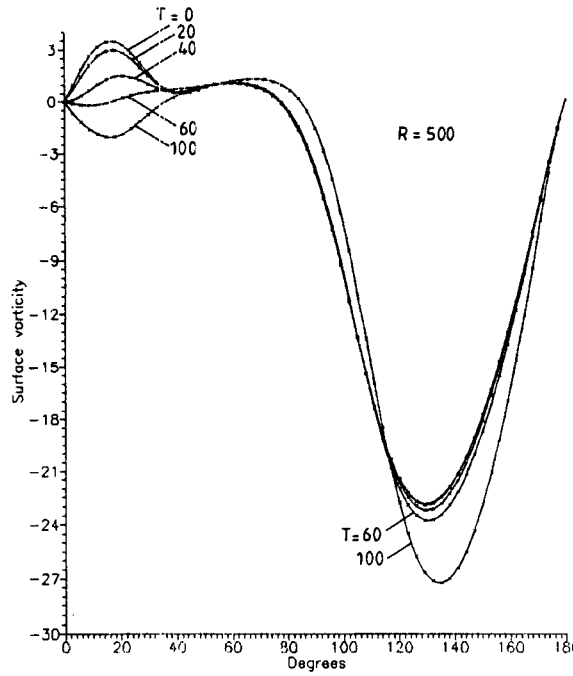


Figure 15. Surface vorticity at $R = 500$

ACKNOWLEDGEMENTS

This investigation was carried out under CSIR project 25/54/90–EMR-II. T.V.S.S. is an SRF in the above project. The authors are grateful to CSIR–EMR- II for financial assistance.

REFERENCES

1. G. I. Taylor, 'The motion of a sphere in rotating liquid', *Proc. R. Soc. Lond. A*, **102**, 180 (1922).
2. R. R. Long, 'Steady motion around a symmetrical obstacle moving axis of a rotating fluid', *J. Met.*, **10**, 197 (1953).
3. T. Maxworthy, 'The flow created by a sphere moving along the axis of a rotating, slightly viscous fluid', *J. Fluid Mech.*, **40**, 453 (1970).
4. C. V. Raghava Rao and T. V. S. Sekhar, 'Numerical solution of the slow translation of a sphere moving along the axis of a rotating viscous fluid', *Int. J. Comput. Fluid Dyn.*, **1**, 351 (1993).
5. J. W. Miles, 'Boundary-layer separation on a sphere in a rotating flow', *J. Fluid Mech.*, **45**, 513 (1971).
6. C. V. Raghava Rao and T. V. S. Sekhar, 'The flow past a spinning sphere in a slowly rotating fluid at small Reynolds numbers—a numerical study', *Int. J. Eng. Sci.*, **31**, 1219 (1993).
7. B. Fornberg, 'Steady viscous flow past a sphere at high Reynolds numbers', *J. Fluid Mech.*, **190**, 471 (1988).
8. S. Leibovich, 'Magnetohydrodynamic flow at a rear stagnation point', *J. Fluid Mech.*, **29**, 401 (1967).
9. J. Buckmaster, 'Separation and magnetohydrodynamics', *J. Fluid Mech.*, **38**, 481 (1969).
10. J. S. Bramely, 'Magnetohydrodynamic flow past a circular cylinder II', *ZAMP*, **26**, 203 (1975).
11. C. V. Raghava Rao and T. V. S. Sekhar, 'Magnetohydrodynamic flow past a circular cylinder—a numerical study', submitted.
12. V. G. Jenson, 'Viscous flow round a sphere at low Reynolds numbers (<40)', *Proc. R. Soc. A*, **249**, 346 (1959).
13. S. C. R. Dennis and J. D. A. Walker, 'Calculation of the steady flow past a sphere at low and moderate Reynolds numbers', *J. Fluid Mech.*, **48**, 771 (1971).
14. S. C. R. Dennis, D. B. Ingham and S. N. Singh, 'The slow translation of a sphere in a rotating viscous fluid', *J. Fluid Mech.*, **117**, 251 (1982).